Ceramics International 47 (2021) 1704–1711

Contents lists available at ScienceDirect

Ceramics International

journal homepage: www.elsevier.com/locate/ceramint

Dielectric and transport properties, electric polarization at the sequential structural phase transitions in iron-substituted bismuth pyrostannate

S.S. Aplesnin [a,b], L.V. Udod [a,b,*], M.N. Sitnikov [b], O.B. Romanova [a]

[a] Kirensky Institute of Physics, Federal Research Center KSC SB RAS, Akademgorodok, 50, Krasnoyarsk, 660036, Russia
[b] Reshetnev Siberian State University of Science and Technology, 660037, Krasnoyarsk, Russia

ARTICLE INFO

Keywords:
Dielectric properties (C)
Impedance (C)
Electrical conductivity (C)
Electric polarization
Thermopower

ABSTRACT

The electrical characteristics including the electrical resistance, impedance, *I–V* characteristics, capacitance, dissipation factor, and thermoelectric power of the $Bi_2Sn_{2-x}Fe_xO_7$ (x = 0.1, 0.2) stannates have been investigated in the temperature range of 100–600 K at frequencies of 10^2–10^6 Hz. The paramagnetic contribution of electrons to the dynamic magnetic susceptibility has been established. The conductivity mechanism of the compounds has been found from the *I–V* characteristics and the change in the carrier sign has been determined from the thermoelectric power . The hysteresis of the *I–V* curves, charge transfer currents and polarization current have been observed in the $Bi_2Sn_{1.8}Fe_{0.2}O_7$ compound. A nonlinear field dependence of the polarization in the orthorhombic phase has been found. The correlation between the obtained characteristics and the phase structure transitions has been established. Two relaxation channels and activation energy have been found using the Debye model. The hysteretic *I–V* characteristics have been explained using a model of the electronic structure and the dipole and migration polarization.

1. Introduction

Bismuth pyrostannate $Bi_2Sn_2O_7$ belongs to the family of compounds with a pyrochlore structure [1] and exhibits the ferroelectric [2] and dielectric [3] properties, superconductivity [4,5], oxygen–ion conductivity [6], colossal magnetoresistance [7], absorption of the radioactive radiation [8], and photocatalysis [9].

Three structural modifications related to the pyrochlore structure are found in polymorphic $Bi_2Sn_2O_7$. Above 900 K, the compound has a cubic structure with minor shifts of Bi^{3+} ions from an ideal pyrochlore structure and belongs to the γ phase [1]. In the temperature range of 390–900 K, the β phase with an orthorhombic structure is realized [10]. At room temperature, the Bi_2Sn_2O7 compound has the non-centrosymmetric monoclinic structure (the α phase) with sp. gr. $P1c1$ [11]. The $Bi_2Sn_2O_7$ structure is well described by two interpenetrating oxide sublattices. The Sn_2O_6 sublattice consists of vertex-sharing SnO_6 octahedra, which form hexagonal rings. In the Bi_2O' sublattice, the Bi^{3+} cation is tetrahedrally coordinated by O′ anions with the O′−A−O′ linear bonds.

It was found that the transitions to the α and β phases are related to the rotation of Bi_2O' tetrahedra, which shift Bi ions to the α phase vertex and to the edge in the β phase of the oxygen octahedron SnO_6 [10]. The correlated Bi^{3+} shifts induce phase transitions to complex ordered structures and change the macroscopic properties.

The binary oxides with a pyrochlore structure undergo a series of low-temperature magnetic and electric phase transitions. In particular, the transitions to the spin-glass state were observed in $Y_2Mo_2O_7$; to the spin-liquid state, in $Tb_2Ti_2O_7$; to the disordered spin-ice state, in $Ho_2Ti_2O_7$ and $Dy_2Ti_2O_7$; to the ordered spin-ice state, in $Tb_2Sn_2O_7$; and to the superconducting state, in $Cd_2Re_2O_7$ [12]. Studies of these physical properties of materials, which are observed at extremely low temperatures, are among the current trends in condensed matter physics.

Oxide compounds containing iron ions are being intensively studied because of their interesting properties. Such, in spinel ferrite $Li_{0.5}Mn_{0.5}Fe_2O_{4-\delta}$ and $Ni_{1.5}Fe_{1.5}O_4$ feature observed the frequency activated conductivity transition from semiconductor to metallic state above 800 K. The conductivity in semiconductor regime has been understood by hopping mechanism of localized charge carriers among the cations in B sites of cubic spinel structure. The charge delocalization process activated a semiconductor-to-metal transition in the ac conductivity curves, obeyed by the Jonscher power law and Drude equation. A metallic state is also confirmed by the frequency dependence of

* Corresponding author. Kirensky Institute of Physics, Federal Research Center KSC SB RAS, Akademgorodok, 50, Krasnoyarsk, 660036, Russia.
E-mail address: luba@iph.krasn.ru (L.V. Udod).

https://doi.org/10.1016/j.ceramint.2020.08.287
Received 21 July 2020; Received in revised form 27 August 2020; Accepted 31 August 2020
Available online 1 September 2020

the dielectric constant curves [27–29]. Electrical conductivity of $Co_{2.75}Fe_{0.25}O_4$ ferrite exhibited a thermal hysteresis loop at high temperatures [30]. The samples α-$Fe_{1.64}Ga_{0.36}O_3$ and Ga-doped Cr_2O_3 system showed a transformation of the I-V curves from linear to non-linear character with the increase of bias voltage, positive magnetoresistance and magnetic field induced negative differential resistance. The magnitudes of critical voltage at which *I-V* curve showed peak and corresponding peak current are affected by magnetic field cycling. The shift of the peak voltage with magnetic field showed a step-wise jump between two discrete voltage levels with least gap (ΔVP) 0.345(± 0.001) V [31, 32]. Temperature variation of the dielectric parameters has shown transformation of the conductivity states (semiconductor ↔ metal like ↔ semiconductor) in the samples of α-$Fe_{1.6}Ga_{0.3}O_3$. Dielectric loss curves indicated coexistence of conduction process and dielectric relaxation process in the samples [33].

Cationic doping changes the pyrochlore structure and the basic physical properties of the compounds, since the structural and physical properties are interrelated. These compounds can be in demand as materials for electrochemical devices and a new generation of electronic devices due to the relatively low synthesis temperatures of doped bismuth titanates and their high thermal stability [13]. The distribution of dopant atoms over two equivalent crystallographic positions increases the variability of properties of the compounds and affects the defectness of the cationic and anionic sublattices, the transport properties of ions (in particular, mobile oxygen O′).

Doping of $Bi_2Ti_2O_7$ bismuth titanate [13] with iron atoms in concentrations of up to 1% narrows a gap in the electron excitation spectrum from 2.83 eV in $Bi_2Ti_2O_7$ to 2.43 eV in $Bi_2Ti_2O_7$, which is attributed to the distribution of iron ions over A and B sites. In the $Bi_2Ti_{2-x}M_xO_7$ (M = V, Cr, Mn, Fe, Ni) [14] compounds with x = 0.5 substituted by d elements in the titanium sites, an impurity level occurs in the band gap. When titanium is replaced by iron, this level is localized closer to the top of the valence band; when it is replaced by chromium, the level is closer to the bottom of the conduction band. Iron-containing bismuth titanates $Bi_{1.6}Fe_xTi_2O_{7-\delta}$ ($x \leq 0.4$) exhibit mainly the electron conductivity.

In $Bi_{1.6}Fe_{0,3}Ti_2O_{7-\delta}$, a transition from the *p*-to *n*-type conductivity upon variation in the oxygen content was detected [15]. At a high partial oxygen pressure, iron-containing bismuth titanate exhibits the hole conductivity; at the low oxygen concentration, the electron conductivity is realized; and, near the minimum conductivity, the ionic contribution is probably added.

The heterovalent replacement of Bi^{3+} and Sn^{4+} ions in the $Bi_2Sn_2O_7$ compound changes the temperature of the α→β transition [1, 16–19] and reduces the crystal symmetry. Substitution of Sn^{4+} ions by Fe^{3+} ones induce crystal lattice distortions and, as the substitute concentration increases, lead to the shift-type structural transitions. In particular, in the $Bi_2(Sn_{1-x}Fe_x)_2O_7$ compound with a concentration of x = 0.2 at T = 140 K, a transition from the monoclinic to triclinic symmetry was detected [20].

The absence of the inversion center in bismuth pyrostannate is a prerequisite for the ferroelectric order at low temperatures. This was confirmed by ab initio theoretical calculations in Ref. [1]. In the $Bi_2(Sn_{0.8}Fe_{0.2})_2O_7$ compound, the magnetoelectric (ME) interaction at temperatures of up to 300 K was detected [21]. An external electric field leads to the crystal lattice distortion and induces the electric polarization. The magnetic field-induced electric polarization is an even function of the magnetic field, except for the range of 140–160 K of the structural phase transition, where the linear ME effect dominates. Upon heating, the magnetic field-induced electric polarization decreases.

In this work, we discuss several problems, including determination of the temperature range of the migration electron polarization, establishing the inductive contribution of electrons to the reactance caused by the space charge in a sample, investigations of the conductivity and carrier types, finding the electric polarization above room temperature, the correlation between the structural phase transitions, and the correlation of the dielectric and transport properties in the $Bi_2(Sn_{1-x}Fe_x)_2O_7$ (x = 0, 0.1, 0.2) compound.

2. Experimental

The $Bi_2Sn_{2-x}Fe_xO_7$ (x = 0.1 and 0.2) compounds were synthesized by the solid-state reaction. The synthesized samples correspond to the monoclinic *Pc* cell in the $Bi_2Sn_2O_7$ α phase [21].

The electrical properties were studied using the four-probe methods on a Keithley 6517B electrometer in the temperature range of 100–600 K. The impedance, capacitance, and dissipation factor were measured with an AM-3028 component analyzer in the frequency range of 1–300 kHz at temperatures of 100–600 K. The thermoelectric voltages on the opposite faces of the sample were detected with an Agilent Technologies 34410A multimeter in the temperature range of 80–500 K.The thermoelectric power was determined on parallelepiped samples by two-contact method. Copper contacts were applied to the ends of the sample. A temperature gradient ΔT = 5K was created along the parallelepiped.

3. Results and discussion

3.1. Permittivity

Fig. 1 shows the temperature dependence of the $Bi_2(Sn_{1-x}Fe_x)_2O_7$ (x = 0.1, 0.2) permittivity. The real part of the permittivity for the sample with x = 0.1 (Fig. 1a) has a maximum at temperatures of about 270–280 K and sharply increases above 500 K. The first the maximum is associated with the localization of electrons at T = 280 K. An increase in ε (T) at 640 K is due to the structural transition with loss of center of inversion. The permittivity change $\varepsilon(T = 280\ K) - \varepsilon(T = 100\ K))/\varepsilon(T = 100\ K)$ at 280 K increases with decreasing frequency and attains 3% at 1 kHz.

The temperature dependences of the imaginary part of the permittivity Im(T) for the sample with x = 0.1 (Fig. 1c) also have anomalies in the form of broad maxima of the dielectric loss in this temperature range. We describe the dielectric susceptibility in the Debye model

$$\mathrm{Re}(\varepsilon) = \varepsilon_0 + \frac{A}{1 + (\omega\tau_1)^2} + \frac{B}{1 + (\omega\tau_2)^2} \quad (1)$$

$$Im(\varepsilon) = \frac{A\omega\tau_1}{1 + (\omega\tau_1)^2} + \frac{B\omega\tau_2}{1 + (\omega\tau_2)^2} \quad (2)$$

where $\tau_{1,2} = \tau_{01,2}\exp(-\Delta E_{1,2}/kT)$ is the relaxation time and ΔE is the activation energy. Fitting to the experimental data yields two energies of $\Delta E_1 = 1700$ K and $\Delta E_2 = 6400$ K.

The temperature dependence of the real part of the permittivity (Fig. 1b) has a maximum at T = 140 K, which confirms the occurrence of a structural transition to the triclinic symmetry [20]. The structural phase transition α→β in the compound with x = 0.2 shifts toward lower temperatures down to T = 350 K. The imaginary part of the permittivity Im(T) for the $Bi_2(Sn_{1-x}Fe_x)_2O_7$ with x = 0.2 (Fig. 1d) hasmaximum in this temperature range and the loss intensity decreases with increasing frequency. These experimental results are consistent with the softening of the IR modes and anomalies in the temperature dependences of the thermal expansion coefficients and sound damping [20]. In the β phase, the transition with the loss of the inversion center at 640 K occurs, which manifests itself in an anomalous increase in the permittivity and is described using the Debye model. At a frequency of 300 kHz, the imaginary part of the permittivity weakly depends from temperature for x = 0.2. This is related with the migration polarization of electrons realized in the frequency band of 10–10^5 Hz.

3.2. Impedance

The capacitive and inductive contributions of carriers in the samples can be estimated by impedance spectroscopy. The temperature

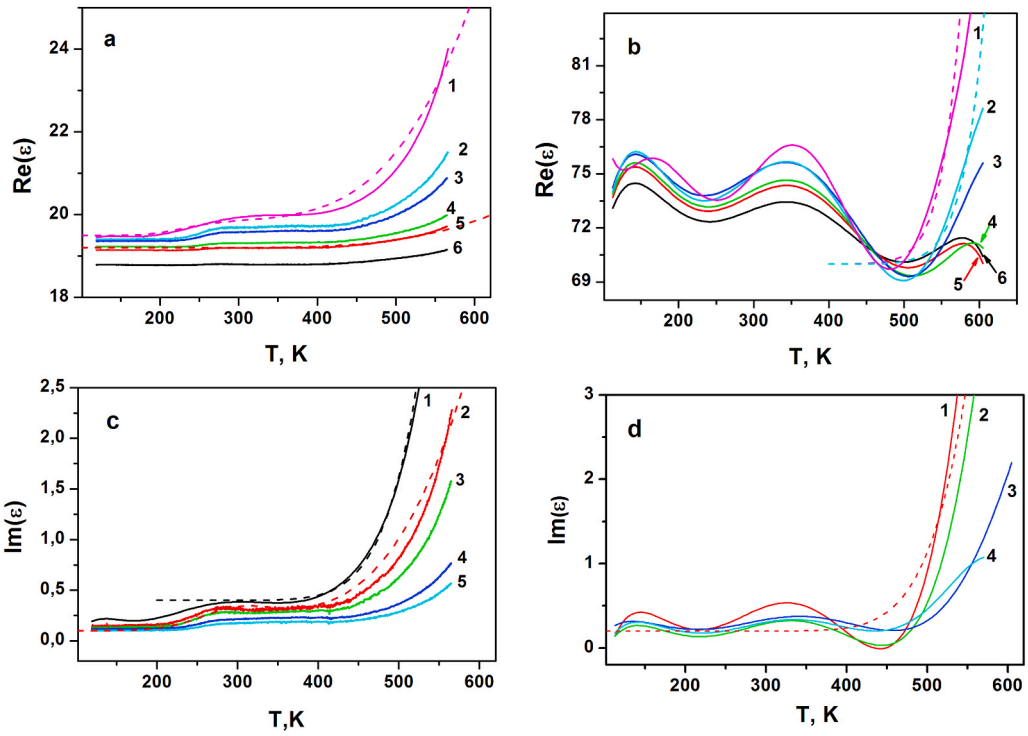

Fig. 1. Temperature dependence of permittivity of $Bi_2(Sn_{1-x}Fe_x)_2O_7$ at different frequencies: (a) real part of permittivity of x=0.1, curve 1 corresponds to 1 kHz, 2 - 5 kHz, 3 - 10 kHz, 4 - 50 kHz, 5 - 100 kHz, 6 - 300 kHz. (b) real part of permittivity of x=0.2, curve 1 corresponds to 1 kHz, 2 - 5 kHz, 3 - 10 kHz, 4 - 50 kHz, 5 - 100 kHz, 6 - 300 kHz. The dashed lines corresponds to functions calculated using the Debye model (1). (c) imaginary part of permittivity of x=0.1, curve 1 corresponds to 1 kHz, 2 - 5 kHz, 3 - 10 kHz, 4 - 50 kHz, 5 - 100 kHz. (d) imaginary part of permittivity of x=0.2, curve 1 corresponds to 5 kHz, 2 - 10 kHz, 3 - 50 kHz, 4 - 100 kHz. The dashed lines corresponds to functions calculated using the Debye model (2).

dependences of the normalized real part of impedance for the $Bi_2(Sn_{1-x}Fe_x)_2O_7$ (x = 0.1 and 0.2) compound are presented in Fig. 2. The temperatures corresponding to the jump in the imaginary part of the impedance Im(Z)/Im (Z (T = 80 K)) by 6–8% at 220 K for the sample with x = 0.1 and the change in the *g* factor coincide (Fig. 2a). At T = 215 K, the *g* factor increases by 1% (inset in Fig. 2a) and the electron spin resonance (ESR) linewidth sharply grows with decreasing temperature [21].

The difference of the temperature behavior of the reactance $X_{L,C}$ from the capacitive resistance X_c (Fig. 2a) points out the inductive contribution, which bring information about the dynamic susceptibility $\chi(\omega)$. In particular, the inductance L is proportional to the magnetic susceptibility (μ): $L \sim \mu = 1 + \chi$ and $\Delta X_L = \chi_\omega(T) - \chi_\omega(T = 80\ K)$. At x = 0.1, the capacitive resistance is almost temperature-independent at high frequencies. When X_L and X_C are connected in series, there is the reactance change $\Delta X_{L,C} = X_L(T) - X_C(T) - X_L(T = 80\ K) - X_C(T = 80\ K) = X_L(T) - X_L(T = 80\ K) = \chi_\omega(T) - \chi_\omega(T = 80\ K)$ caused by an increase in the dynamic magnetic susceptibility due to the appearance of electrons on the Fermi surface and the paramagnetic contribution. The Pauli susceptibility is temperature-independent, which is in qualitative agreement with the experimental data. The reactance jump at 360 K is caused by an increase in the electron density on the Fermi surface by 1%.

The imaginary part of the impedance of the $Bi_2(Sn_{1-x}Fe_x)_2O_7$ (x = 0.2) sample has a minimum Z''/Z'' (T = 80 K) in the vicinity of T_{min} = 310 K and its value decreases with increasing frequency by two orders of magnitude. The temperature T_{min} weakly depends on frequency. In the temperature range of 260–310 K, the impedance decreases due to the inductance, because the capacitance is almost temperature-independent in this range. The localization of electrons in this temperature range leads to a decrease in the electron density on the Fermi surface and in the contribution to the paramagnetic susceptibility $X_{(L,C)} = \chi_\omega(T) - \chi_\omega(T = 80\ K) \sim -0.03$. This is confirmed by the presence of a broad maximum in the temperature dependence of the active resistance (Fig. 3b) at 260–340 K. Heating to 400 K leads again to the carrier of charges localization, an increase in the capacitance, independence of the resistance of the temperature, and a decrease in the paramagnetic contribution of electrons to the magnetic susceptibility. Such an unusual temperature behavior of the impedance is related to the presence of

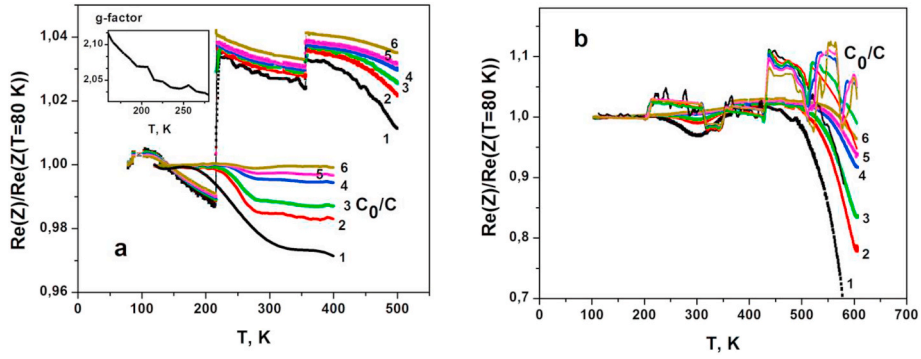

Fig. 2. Temperature dependence of the reduced impedance and reduced capacitance $Bi_2(Sn_{1-x}Fe_x)_2O_7$. (a) x = 0.1, curve 1 corresponds to 1 kHz, 2–5 kHz, 3–10 kHz, 4–50 kHz, 5–100 kHz, 6–300 kHz. The inset shows the temperature dependence of the g factor for x = 0.1. (b) x = 0.2, curve 1 corresponds to 1 kHz, 2–5 kHz, 3–10 kHz, 4–50 kHz, 5–100 kHz, 6–300 kHz.

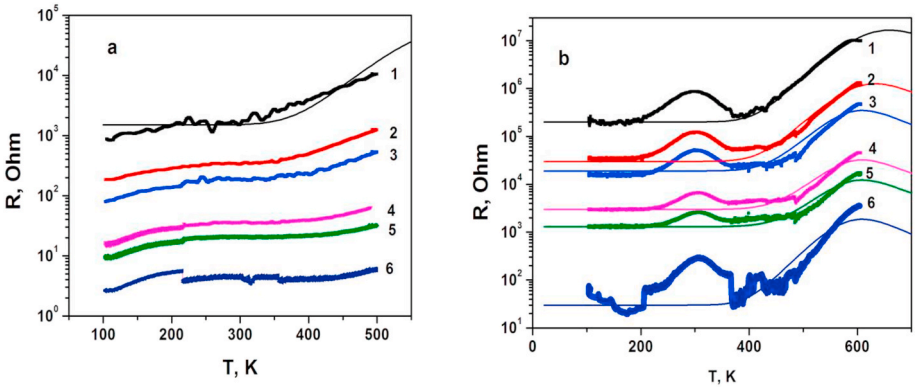

Fig. 3. Temperature dependence of ac resistance of $Bi_2(Sn_{1-x}Fe_x)_2O_7$. (a) x = 0.1, curve 1 corresponds to 1 kHz, 2–5 kHz, 3–10 kHz, 4–50 kHz, 5–100 kHz, 6–300 kHz. (b) x = 0.2, curve 1 corresponds to 1 kHz, 2–5 kHz, 3–10 kHz, 4–50 kHz, 5–100 kHz, 6–300 kHz. The dashed lines correspond to theoretical calculations (3).

polymorphic transitions and the coexistence of crystalline domains of different phases where carriers of charges are localized.

Upon substitution of tin ions by iron, the transition α→β is extended in temperature. Some domains containing iron ions start passing to the β phase at T = 350 K [20]. Above 460 K, a decrease in the impedance of the $Bi_2(Sn_{1-x}Fe_x)_2O_7$ (x = 0.1, 0.2) samples is related to an increase in the capacitance by the expense of the relaxation conductivity.

The temperature dependences of the ac resistance for the $Bi_2(Sn_{1-x}Fe_x)_2O_7$ (x = 0.1, 0.2) compound at several frequencies from 1 to 300 kHz are presented in Fig. 3. The active resistance for the sample with x = 0.1 has small jumps at a temperature of T = 220 K and, for the sample with x = 0.2, there is a broad maximum in the range of 260–360 K (Fig. 3b). The temperatures of the R(T) and permittivity maxima coincide and are caused by the stage-by-stage transition of the compound into the β phase. In the same temperature range, the IR modes at frequencies of 510–540 cm^{-1}, which are related to the vibrations of the Bi–O′ bond, are softened [20].

At high temperatures, the ac resistance of the compositions with two concentrations sharply increases. The active resistance characterizes the absorption of electromagnetic radiation and can be described using the Debye model as

$$Re(Z) = \frac{A\omega\tau}{1 + (\omega\tau)^2} \quad (3)$$

where the relaxation time obeys the Arrhenius law $\tau = \tau_0 \exp(-\Delta E/kT)$ with ΔE = 6400 K. The maximum adsorption is obtained in the proximity of the phase transition with the loss of the inversion center, which is indicated by the differential scanning calorimetry data (DSC) for the $Bi_2(Sn_{1-x}Cr_x)_2O_7$ (x = 0–0.1) samples. The DSC study shows the diffuse exo- and endo-effects around 600 and 646 K [22]. The Debye model satisfactorily describes the temperature dependence of the resistance above 400 K. The maxima in the theoretical curves at T > 600 K correspond to the phase transition with the loss of the inversion center. The temperature T_{max} increases with frequency [20].

3.3. *I–V characteristics and conductivity*

The dc electric properties of the $Bi_2(Sn_{1-x}Fe_x)_2O_7$ compound were examined by the two-probe method using an Agilent Technologies 344 10A multimeter at temperatures of 100–700 K. Both compositions exhibit the semiconductor-type conductivity with a decrease of the electrical resistance by four orders of magnitude upon heating. The R(T) dependence for the $Bi_2(Sn_{1-x}Fe_x)_2O_7$ (x = 0.1) sample has anomalies (Fig. 4a) at temperatures of 124–140, 229, 300, 448, and 517 K. The first anomaly is induced by the change of the crystal lattice structure and the transition from the triclinic to monoclinic structure. The maximum at T = 229 K is consistent with the anomalies of the thermal expansion coefficient β(T) and the softening of frequency in the IR spectra [20].

The next anomalies at T = 300 and 448 K can be explained by the domain crystal structure observed in the $Bi_2Sn_2O_7$ compound at room temperature [1]. Using the linear dependence of the resistance logarithm on the reciprocal temperature $\lg\rho = \lg\rho_0 + (\Delta E/k_B T)$, we calculated the activation energy and its growth from ΔE = 0.3 eV at 300–450 K to ΔE = 1.2 eV at 500–700 K in the composition with x = 0.1.

The electrical resistance of the $Bi_2(Sn_{1-x}Fe_x)_2O_7$ (x = 0.2) sample (Fig. 5b) sharply decreases upon heating above 220 K with an activation energy of ΔE = 0.23 eV in the temperature range of 220–320 K. In the temperature range of 310–390 K, several anomalies are observed, which are consistent with the nucleation of β phase domains containing iron ions.

We establish the $Bi_2(Sn_{1-x}Fe_x)_2O_7$ conductivity mechanism from the *I–V* characteristics measured in external electric fields ranged from −800 to 800 V/cm at temperatures of 300–600 K. The conductive

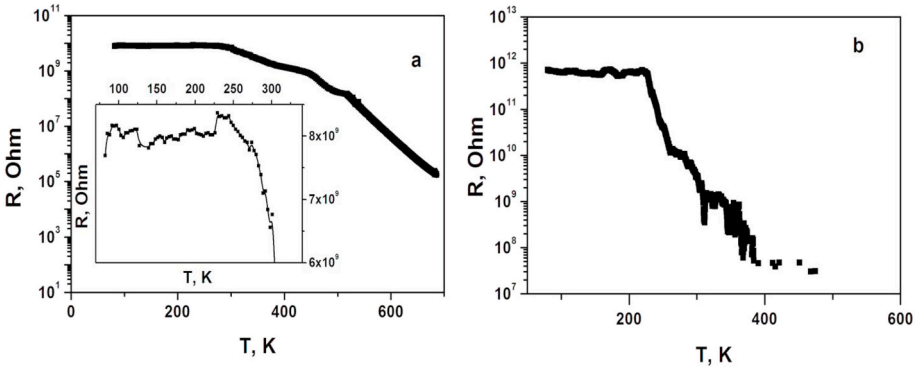

Fig. 4. Temperature dependence of dc resistance of $Bi_2(Sn_{1-x}Fe_x)_2O_7$. (a) x = 0.1, (b) x = 0.2.

current increases with the iron concentration. At x = 0.1, the dependence of the current flowing through the sample on the applied voltage has a symmetric shape. Fig. 5 shows the *I–V* characteristic for the $Bi_2(Sn_{1-x}Fe_x)_2O_7$ (x = 0.1) sample. At low temperatures, the scattering of carriers is induced by charged intrinsic defects and the conductivity is described by the quadratic Mott law with a variable jump length [16, 23–24]

$$j = \frac{9}{8}\tau_\mu \sigma_0 \mu \frac{U^2}{L^3} \quad (4)$$

where j is the current density, τ_μ is the Maxwell relaxation time, σ_0 is the electrical conductivity in the bulk of the material without injection of carriers, μ is the carrier mobility, U is the applied voltage, and L is the sample thickness.

Upon heating above 400 K in the orthorhombic β phase, the conductivity type changes from Mott to ohmic. The change of the conduction mechanism at x = 0.1 is consistent with the change of the charge carrier activation energy.

The *I–V* characteristics of the $Bi_2(Sn_{1-x}Fe_x)_2O_7$ (x = 0.2, 0.1) samples are qualitatively different. This difference is caused by the formation of the electric polarization and ME interaction in the $Bi_2(Sn_{0.8}Fe_{0.2})_2O_7$ compound [21]. The *I–V* characteristics for the composition with x = 0.2 has a hysteresis shifted along the voltage and current axes (Fig. 6a and b). The electric bias field (inset in Fig. 6a) induced by the nonuniform distribution of defects over the anionic subsystem of the sample and decreases by a factor of 4–5 at T = 550 K. In the $CaMnO_{3-\delta}$ and $Ca_{1-y}Re_yMnO_3$ manganites [25–26] with the nonstoichiometric substitution, oxygen vacancies at these temperatures are ordered.

The *I–V* hysteresis originates from the ferroelectric polarization induced by the polar Bi–O bond with an unshared electron pair on a bismuth ion. The total current passing through the sample consists of the charge transport current I_{ch} and the polarization current I_p: $I = I_{ch} + I_p$. The transport current obeys the Ohm's law $I_{ch} = U/R$ at $T \geq 500$ K (the dashed line in Fig. 6b) and nonlinearly depends from voltage at T < 500 K (the dotted line in aFig. 6). The polarization current is $I_p = dP/dt$. Thus, we have $I = U/R + I_p$ and the polarization current $I_p = I - I_{ch}$ passes through the maximum in the voltage range of ($-U_{min}$–U_{max}) (cFig. 6, d). We determine the voltage dependence of the electric polarization using the relation $j = dP/dt = (dP/dU)\,(dU/dt)$, where $P = \int jdU/\left(\frac{dU}{dt}\right)$, accurate to a constant factor.

The *I–V* characteristics were measured for 100 s at the linear time

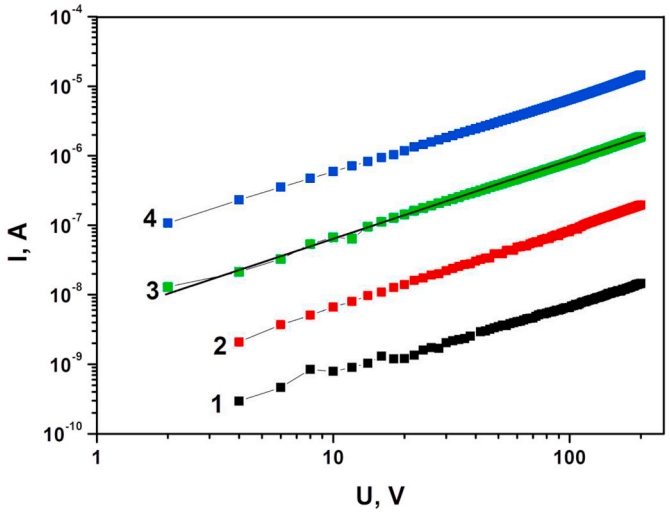

Fig. 5. I–V characteristics of $Bi_2(Sn_{1-x}Fe_x)_2O_7$, x = 0.1 in zero magnetic field. The curve 1 corresponds to the I – V characteristic measured at 450 K, 2–500 K, 3–550 K, 4–600 K.

dependence of the voltage: $U = -U_{min} + at$. The current increases linearly also: $I_{ch} = -I_{max} + at$, where I_{max} is the maximum current and t is the time during which the voltage increases from $-U_{min}$ to U_{max}. The polarization current obeys the harmonic law $I_p = I_{pmax} \cos(\omega t + \varphi)$ (Fig. 6c), where ω = 1/T, T is the time of the measurements of the *I–V* characteristic, and φ is the phase. The electric polarization hysteresis (Fig. 7) and the phase shift between the external field and the polarization current are not observed up to T = 550 K. At temperatures of T = 550 and 600 K, there are the hysteresis in the P(U) dependence (Fig. 7b) and the phase shift between the current polarization and external field (Fig. 6d). In the sample, the displacement of the boundary of the electric polarization region lags in phase behind the external electric field.

Above room temperature, the electric polarization increases as a result of the occurrence of an additional contribution of migration polarization of electron (Fig. 7). Due to the interaction of dipole and migration polarizations, the change in the polarization current lags in phase behind the external electric field.

3.4. Thermoelectric power

We determine the position of the impurity subband relative to the valence band and the type of current carrier from the thermopower S(T) measured in the temperature range of 80–500 K. Fig. 8 shows the temperature dependence of the thermopower coefficient for the $Bi_2(Sn_{1-x}Fe_x)_2O_7$ (x = 0.1, 0.2) samples. The S(T) dependence for the composition with x = 0.1 changes its sign twice at temperatures of 115 and 415 K, which points out the change of the conductivity type. In the $Bi_2(Sn_{0.8}Fe_{0.2})_2O_7$ compound, the thermopower coefficient is positive and the S(T) curve has two maxima at T = 135 and 345 K. Both maxima are located near structural phase transitions: the first maximum corresponds to the transition from the monoclinic to a triclinic structure; the second to the α → β transition. The temperature of maximum (T = 354 K) in the S(T) curve for the composition with x = 0.1 coincides with the temperatures of the impedance jump and softening of the stretching mode in the MeO_6 octahedron [21], as well as with the maximum of the electrical resistance derivative (dR/dT)/R (inset in).

Substitution of Sn^{4+} ions for Fe^{3+} ones leads to the formation of acceptor levels near the valence band. The distortion of the oxygen octahedra causes a shift of the valence band and a change in the spectral density of states. Nonstoichiometric substitution leads to the formation of a hole in the anion subsystem and the strong electron–phonon interaction. As the crystal symmetry increases, the gap in the electron excitation spectrum and the impurity subband width increase in the β phase due to dissociation of a lattice polaron. The formation of β-phase domains causes the band bending and the transition of electrons from the valence band of the α phase to the impurity subband of the β phase (Fig. 9). The potential difference $\varphi_\alpha - \varphi_\beta$ is induced between domains. The energy flow j_E is transferred by charged particles: $j_E \sim j_N$. The charged particle flow $j_N = D\,dN/dx$ is determined by the diffusivity $D \sim v\,\lambda = v^2 \cdot \tau$, where v is the velocity and τ is the relaxation time. In the relaxation time approximation, the thermopower is $S \sim D \sim v^2 \cdot \tau$. The relaxation time in the proximity of the phase transition is determined by the power dependence $\tau \sim 1/(T - T_c)^{z\nu}$, where T_c is the transition temperature and z and ν are the critical indices. In the $Bi_2(Sn_{1-x}Fe_x)_2O_7$ solid solutions, the phases coexist and therefore the phase transition is diffuse and extended in temperature by ΔT. The experimental data are well described by the function:

$$S = \frac{A}{(abs(T - T_c) + \Delta T)} \quad (5)$$

where ΔT = 50 K at x = 0.1 and 20 and 40 K at x = 0.2. Upon heating, the volume fraction of the β phase increases; above 415 K, the volume is $V_\beta > V_\alpha$, the impurity subband of the β phase is filled with electrons, and its potential exceeds that of the α phase. As a result, the thermoelectric current changes its sign. This model explains the change in the

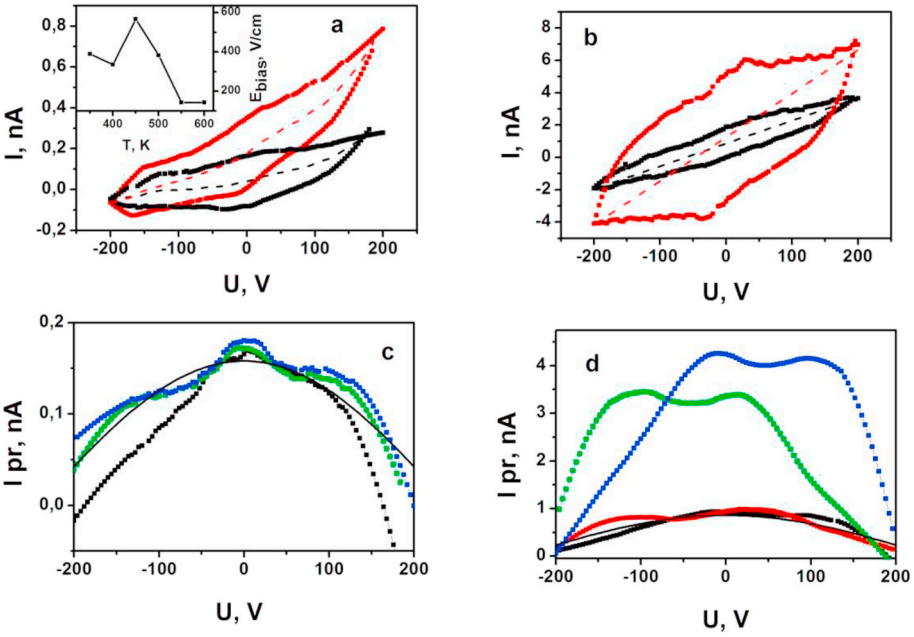

Fig. 6. I–V characteristics of Bi2(Sn1-xFex)2O7, x = 0.2. (a) Curve 1 corresponds to T = 350 K, 2–450 K, The inset shows the temperature dependence of the electric bias field. (b) Curve 1 corresponds to T = 500 K, 2–550 K. Current with charge transfer (dashed line). (c) Polarization current, curve 1 corresponds to T = 350 K with a decrease in voltage from 200 V to −200 V, 2- T = 450 K with a decrease in voltage from 200 V to −200 V, 3- T = 450 K with an increase in voltage from - 200 V to 200 V, the solid line corresponds to the fitting function $I_p = I_{p0} \cos(\omega t + \phi)$ with $\phi = 0$. (d) Polarization current: curve 1 corresponds to T = 500 K with decreasing voltage from 200 V to −200 V, 2- T = 500 K with increasing voltage from −200 V to 200 V, 3-T = 550 K with increasing voltage from - 200 V to 200 V, 4 - T = 550 K with voltage reduction from 200 V to −200 V. Fitting function $I_p = I_{p0} \cos(\omega t)$ (solid line).

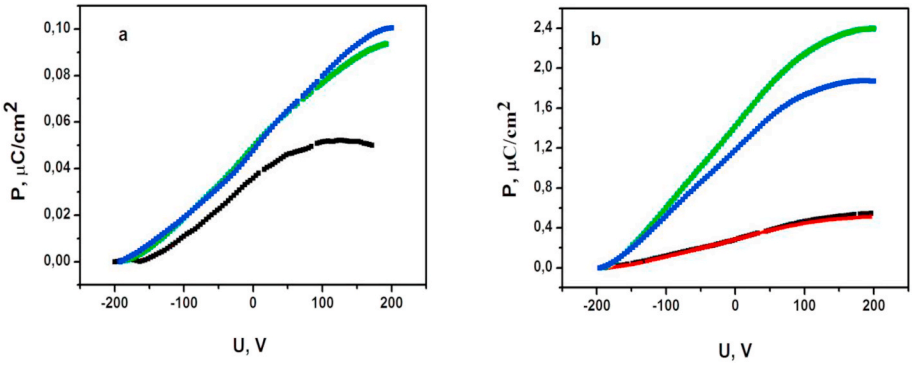

Fig. 7. Dependence of the electric polarization from the applied electric field $Bi_2(Sn_{1-x}Fe_x)_2O_7$. (a) x = 0.1, curve 1 corresponds to T = 350 K with decreasing voltage from 200 V to −200 V, 2- T = 450 K with decreasing voltage from 200 V to −200 V, 3- T = 450 K with increasing voltage from −200 V to 200 V. (c) x = 0.2, curve 1 corresponds to T = 500 K with decreasing voltage from 200 V to −200 V, 2- T = 500 K with increasing voltage from 200 V to −200 V, 3 - T = 550 K with increasing voltage from −200 V to 200 V, 4- T = 550 K with decreasing voltage from 200 V to −200 V.

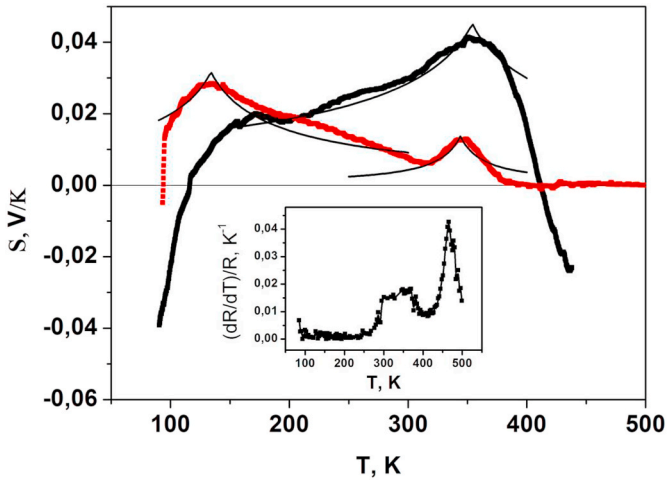

Fig. 8. Temperature dependence of the thermopower coefficient of $Bi_2(Sn_{1-x}Fe_x)_2O_7$. Curve 1 corresponds to x = 0.1, 2- x = 0.2. Solid lines represent the theoretical calculations (4). The inset shows (dR/dT)/R for x = 0.1.

thermopower sign below the temperature of the structural transition from the monoclinic to triclinic crystal structure.

4. Conclusions

It was shown that, in bismuth pyrostannate $Bi_2(Sn_{1-x}Fe_x)_2O_7$ (x = 0.1), the change in the *g* factor at 220 K is related to the inductive contribution of electrons to the impedance and with an increase in Pauli contribution to the paramagnetic susceptibility. The permittivity anomaly at 280 K is caused by the localization of carriers of current. Above this temperature, the conductivity has an activation character. In the vicinity of 360 K, the extended transition α→β with the coexisting phases was found, which is accompanied by the thermopower maximum and an increase in the dynamic paramagnetic susceptibility. In the β phase, the conductivity type changes from Mott to ohmic and the type carrier of current changes from hole to electron.

In the $Bi_2(Sn_{0.8}Fe_{0.2})_2O_7$ compound with the ME interaction, the inductive contribution to the impedance was found near the change of the conductivity type from tunnel to activation and in the orthorhombic β phase. The phase transitions from the triclinic to monoclinic structure, the transition α→β, and the transition from the noncentrosymmetric to centrosymmetric structure are accompanied by the maxima in the temperature dependences of the permittivity and thermopower. The *I–V* hysteresis, charge transport current, and polarization current were

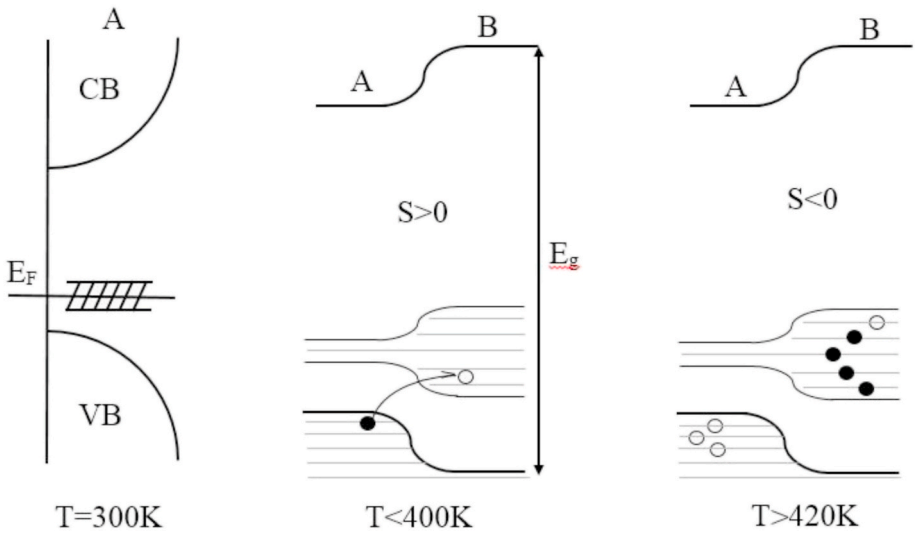

Fig. 9. Model diagram of energy levels. VB is the valence band, CB is the impurity band, A – is the α phase, B – is the β phase, S is the thermopower coefficient, E_F is the Fermi level, E_g is the band-gap.

found. The critical temperature of the sharp drop of the bias field was found, below which the polarization current coincides in phase with the external field. A nonlinear dependence of the electric polarization as a function of the field with the absence of hysteresis in the β phase was established and attributed to the interaction between the dipole and migration polarizations. A model of the electronic structure was proposed.

Declaration of competing interest

The authors declare that they have no known competing financial interests or personal relationships that could have appeared to influence the work reported in this paper.

Acknowledgements

The reported study was funded by Russian Foundation for Basic Research project N☺ 20-52-00005 Bel_a.

References

[1] R.D. Shannon, J.D. Bierlein, J.L. Gillson, G.A. Jones, A.W. Sleight, Polymorphismin $Bi_2Sn_2O_7$, J. Phys. Chem. Solid. 41 (1980) 117–122, https://doi.org/10.1016/0022-3697(80)90041-4.
[2] W.R. Cook Jr., H. Jaffe, Ferroelectricity in oxides of fluorite structure, Phys. Rev. 88 (1952) 1426.
[3] E. Buixaderas, S. Kamba, J. Petzelt, Lattice dynamics and central-mode phenomena in the dielectric response of ferroelectrics and related materials, Ferroelectrics 308 (2004) 131–192, https://doi.org/10.1080/00150190490508909.
[4] M. Hanawa, Y. Muraoka, T. Tayama, T. Sakakibara, J. Yamaura, Z. Hiroi, Superconductivity at 1 K in $Cd_2Re_2O_7$, Phys. Rev. Lett. 87 (2001) 187001, https://doi.org/10.1103/PhysRevLett.87.187001.
[5] A.W. Sleight, J.L. Gillson, Platinum metal pyrochlores of the type $Tl_2M_2O_7$, Mater. Res. Bull. 6 (1971) 781–784, https://doi.org/10.1016/0025-5408(71)90114-0.
[6] M.P. van Dijk, K.J. de Vries, A.J. Burggraaf, Oxygen ion and mixed conductivity in compounds with the fluorite and pirochlore strucrure, Solid State Ionics 9–10 (1983) 913–920.
[7] M.A. Subramanian, B.H. Toby, A.P. Ramirez, W.J. Marshall, A.W. Sleight, G. H. Kwei, Colossal magnetoresistance without Mn^{3+}/Mn^{4+} double exchange in the stoichiometric pyrochlore $Tl_2Mn_2O_7$, Science 273 (1996) 81–84, https://doi.org/10.1126/science.273.5271.81.
[8] N.P. Laverov, S.V. Yudintsev, T.S. Livshits, S.V. Stefanovsky, A.N. Lukinykh, R. C. Ewing, Synthetic minerals with the pyrochlore and garnet structures for immobilization of actinide-containing wastes, Geochem. Int. 48 (2010) 1–14, https://doi.org/10.1134/s0016702910010015.
[9] O. Merka, D.W. Bahnemann, M. Wark, Photocatalytic hydrogen production with non-stoichiometric pyrochlore bismuth titanate, Catal. Today 225 (2013) 102–110, https://doi.org/10.1016/j.cattod.2013.09.009.
[10] James W. Lewis, Julia L. Payne, Ivana Radosavljevic Evans, Harold T. Stokes, Branton J. Campbell, John S.O. Evans, An exhaustive symmetry approach to structure determination: phase transitions in $Bi_2Sn_2O_7$, J. Am. Chem. Soc. 138 (2016) 8031–8042, https://doi.org/10.1021/jacs.6b04947.
[11] I. Radosavljevic Evans, J.A.K. Howard, J.S.O. Evans, α-$Bi_2Sn_2O_7$ – a 176 atom crystal structure from powder diffraction data, J. Mater. Chem.J. Mater. Chem. 13 (2003) 2098–2103.
[12] J.S. Gardner, M.J.P. Gingras, J.E. Greedan, Magnetic pyrochlore oxides, Rev. Mod. Phys. 82 (2010) 53–107, https://doi.org/10.1103/revmodphys.82.53.
[13] S. Murugesan, M.N. Huda, Y. Yan, M.M. Jassim, V.(R.) Subramanian, Band-engineering bismuth titanate pyrochlores for visible light photocatalysis, J. Phys. Chem. C 114 (2010) 10598–10605, https://doi.org/10.1021/jp906252r.
[14] B. Allured, S. Dela Cruz, T. Darling, M.N. Huda, V.(R.) Subramanian, Enhancing the visible light absorbance of $Bi_2Ti_2O_7$ through Fe-substitution and its effects on photocatalytic hydrogen evolution, Appl. Catal. A: Environmental. 144 (2014) 261–268, https://doi.org/10.1016/j.apcatb.2013.07.019.
[15] V.N. Chebotin, M.V. Perfiliev, Electrochemistry of Solid Electrolytes, M.: Chemistry, 1978, p. 312P.
[16] S.S. Aplesnin, L.V. Udod, M.N. Sitnikov, N.P. Shestakov, $Bi_2(Sn_{0.95}Cr_{0.05})_2O_7$: structure, IR spectra, and dielectric properties, Ceram. Int. 42 (2016) 5177–5183, https://doi.org/10.1016/j.ceramint.2015.12.040.
[17] S.S. Aplesnin, L.V. Udod, M.N. Sitnikov, Electronic transition, ferroelectric and thermoelectric properties of bismuth pyrostannate $Bi_2(Sn_{0.85}Cr_{0.15})_2O_7$, Ceram. Int. 44 (2018) 1614–1620, https://doi.org/10.1016/j.ceramint.2017.10.082.
[18] S.S. Aplesnin, L.V. Udod, M.N. Sitnikov, V.V. Kretinin, M.S. Molokeev, N. Mironova-Ulmane, Dipole glass in chromium-substituted bismuth pyrostannate, Mater. Res. Express 5 (2018) 115202, https://doi.org/10.1088/2053-1591/aaddd9.
[19] S.S. Aplesnin, L.V. Udod, M.N. Sitnikov, M.S. Molokeev, L.S. Tarasova, K. I. Yanushkevich, Magnetic, dielectric, and transport properties of bismuth pyrostannate $Bi_2(Sn_{0.9}Mn_{0.1})_2O_7$, Phys. Solid State 59 (2017) 2268–2273, https://doi.org/10.21883/FTT.2017.11.45069.125.
[20] L.V. Udod, S.S. Aplesnin, M.N. Sitnikov, O.B. Romanova, M.N. Molokeev, Phase transitions in bismuth pyrostannate upon substitution of tin by iron ions, J. Alloys Compd. 804 (2019) 281–287, https://doi.org/10.1016/j.jallcom.2019.07.020.
[21] L.V. Udod, S.S. Aplesnin, M.N. Sitnikov, O.B. Romanova, O.A. Bayukov, A. M. Vorotinov, D.A. Velikanov, G.S. Patrin, Magnetodielectric Effect and Spin State of Iron Ions in Substituted Bismuth Pyrostannate, EPJP, 2020 in press.
[22] S.S. Aplesnin, L.V. Udod, M.N. Sitnikov, E.V. Eremin, M.S. Molokeev, L. S. Tarasova, K.I. Yanushkevich, A.I. Galyas, Correlation of the magnetic and transport properties with polymorphic transitions in bismuth pyrostannate $Bi_2(Sn_{1-x}Cr_x)_2O_7$, Phys. Solid State 57 (2015) 1627–1632, https://doi.org/10.1134/S1063783415080028.
[23] N.F. Mott, E.F. Davis, Electronic Processes in Non-crystalline Materials, Oxford, 1971.
[24] S.S. Aplesnin, L.V. Udod, Y.Y. Loginov, V.V. Kretinin, A.N. Masyugin, IOP Conf. Ser. Mater. Sci. Eng. 467 (2019), 012014, https://doi.org/10.1088/1757-899X/467/1/012014.
[25] E.V. Mostovshchikova, N.N. Loshkareva, B.A. Gizhevskii, N.I. Solin, A. M. Balbashov, Charge carriers in optical spectra of electron-doped $Ca_{1-x}La_xMnO_3$ single crystals, J. MMM 300 (2006) e147–e150, https://doi.org/10.1016/j.jmmm.2005.10.170.
[26] K.R. Poeppelmeier, M.E. Leonowicz, J.M. Longo, $CaMnO_{2.5}$ and $Ca_2MnO_{3.5}$: new oxygen-defect perovskite-type oxides, Solid St. Chem. 44 (1982) 89–98.
[27] R.N. Bhowmika, G. Vijayasri, Study of microstructure and semiconductor to metallic conductivity transition in solid state sintered $Li_{0.5}Mn_{0.5}Fe_2O_{4-\delta}$ spinel ferrite, J. Appl. Phys. 114 (2013) 223701, https://doi.org/10.1063/1.4845895, 13.

[28] R.N. Bhowmik, Temperature- and frequency-activated semiconductor-to-metal transition in soft ferromagnetic $Li_{0.5}Mn_{0.5}Fe_2O_4$ ferrite, Mater. Res. Express 1 (2014) 015903, https://doi.org/10.1088/2053-1591/1/1/015903.
[29] R.N. Bhowmik, K.S.A. Kumar, Role of pH value during material synthesis and grain-grain boundary contribution on the observed semiconductor to metal like conductivity transition in $Ni_{1.5}Fe_{1.5}O_4$ spinel ferrite, Mater. Chem. Phys. 177 (2016) 417e428, https://doi.org/10.1016/j.matchemphys.2016.04.048.
[30] R.N. Bhowmik, P.D. Babu, A.K. Sinha, A. Bhisikar, High-temperature thermal cycling effect on the irreversible responses of lattice structure, magnetic properties, and electrical conductivity in $Co_{2.75}Fe_{0.25}O_{4+\delta}$ spinel oxide, Inorg. Chem 59 (2020) 6763–6773, https://doi.org/10.1021/acs.inorgchem.9b03755.
[31] R.N. Bhowmika, G. Vijayasri, Magnetic field cycling effect on the non-linear current-voltage characteristics and magnetic field induced negative differential resistance in α-$Fe_{1.64}Ga_{0.36}O_3$ oxide, AIP Adv 5 (2015) 067126, https://doi.org/10.1063/1.4922511.
[32] R.N. Bhowmik, K.V. Siva, Non-equilibrium character of resistive switching and negative differential resistance in Ga-doped Cr_2O_3 system, JMMM 457 (2018) 17–29, https://doi.org/10.1016/j.jmmm.2018.02.070.
[33] R.N. Bhowmik, A.G. Lone, Dielectric properties of a-$Fe_{1.6}Ga_{0.4}O_3$ oxide: A promising magnetoelectric material, J. Alloys Compd. 680 (2016) 31e42, https://doi.org/10.1016/j.jallcom.2016.04.058.